An investigation into energy harvesting and storage to power a more electric regional aircraft

Ahmed Saleh[1], Constantina Lekakou[*1] and John Doherty[2]

[1]*Centre for Engineering Materials, Department of Mechanical Engineering Sciences,
University of Surrey, Guildford, GU2 7XH, U.K.*
[2]*Centre for Aerodynamics and Environmental Flow, Department of Mechanical Engineering Sciences,
University of Surrey, Guildford, GU2 7XH, U.K.*

Abstract. This is an investigation for a more electric regional aircraft, considering the ATR 72 aircraft as an example and the electrification of its four double slotted flaps, which were estimated to require an energy of 540 Wh for takeoff and 1780 Wh for landing, with a maximum power requirement of 35.6 kW during landing. An analysis and evaluation of three energy harvesting systems has been carried out, which led to the recommendation of a combination of a piezoelectric and a thermoelectric harvesting system providing 65% and 17%, respectively, of the required energy for the actuators of the four flaps. The remaining energy may be provided by a solar energy harvesting photovoltaic system, which was calculated to have a maximum capacity of 12.8 kWh at maximum solar irradiance. It was estimated that a supercapacitor of 232 kg could provide the energy storage and power required for the four flaps, which proved to be 59% of the required weight of a lithium iron phosphate (LFP) battery while the supercapacitor also constitutes a safer option.

1. Introduction

Recent developments along the vision for an electric aircraft move towards a more electric aircraft (MEA) (Trinklein *et al.* 2020, Moore and Ning 2019), air microvehicles (Hudson *et al.* 2020) and unmanned aerial vehicles (Matlock *et al.* 2019). Within the concept of an MEA, the present study considers the electrification of the flaps actuator system in a regional aircraft. A case study is developed around the ATR 72, a 70 passenger, twin-engine turboprop aircraft, which has been recently considered as a basis for the development of hybrid-electric propulsion systems (Jux *et al.* 2018, Voskuijl *et al.* 2018). After analyzing 6000 flights of four ATR 72 aircraft, Jux *et al.* (2018) determined a median flight time of 60 minutes, an average travelled distance of 407 km (out of 1500 km range), an average required power at 53% of the maximum power, and a maximum required power duration of 52 seconds during takeoff and climb phases of the flight. In the current ATR 72 models, the flaps are actuated hydraulically and the ailerons are actuated electromechanically (ATR Systems 2010). There are currently two hydraulic actuation systems, of

---

∗Corresponding author, Ph.D., E-mail: c.lekakou@surrey.ac.uk

which the blue system caters for the flaps, the spoilers, the nose wheel steering and the brakes. The two hydraulic systems are fed by a common hydraulic tank containing 8.5 lt of fluid (4 lt for each system), which weighs about 7.5 kg of hydraulic fluid; they are pressurized by an ACW electric motor driven pump operating at a typical pressure of 3000 psi (ATR 72 Flight crew operating manual 1999). Replacing the hydraulic system by electromechanical actuators in aircraft, not only brings gains in weight, volume and energy efficiency, but also significant advantages in safety and maintenance, as hydraulic systems leak and hydraulic fluids are flammable and toxic, generating toxic fumes (Qiao *et al.* 2018).

The present study is seeking to provide an electric power system for the four flaps of the ATR 72 aircraft, consisting of an energy harvesting and an energy storage system. Three options of energy harvesting will be investigated: (a) photovoltaics for solar energy harvesting; (b) thermoelectric energy harvesting and (c) piezoelectric energy harvesting.

Lightweight thin film photovoltaics (PVs) include amorphous silicon thin film solar cells with an efficiency of 5-8% (Söderström *et al.* 2008), cadmium telluride and copper indium gallium diselenide photovoltaics, with the last two categories having an efficiency around 9-10% (Kim *et al.* 2012) at module level. Compared to 20% and 25% efficiency of the polycrystalline and monocrystalline silicon PVs, respectively, the thin film PVs have clearly lower efficiency but their low weight makes them ideal for aircraft applications.

Thermoelectric materials are characterized by the Z factor which is proportional to the electrical conductivity and the square power of the Seebeck coefficient and inversely proportional to the thermal conductivity. Bismuth telluride alloys may reach a maximum Z= 3-3.3 $\times 10^{-3}$ K^{-1} at room temperature (Andre *et al.* 2009 Lim *et al.* 2017). Polymers have generally lower Z factor, although P3HT-rich P3HT:PCBM p-type and PCBM-rich P3HT:PCBM n-type devices have reached Z = 3.4$\times 10^{-3}$ K^{-1} (Xu *et al.* 2013, Pope and Lekakou 2019).

Piezoelectric materials convert vibration energy to electric energy. Their characteristic properties include the piezoelectric coefficients **d** matrix (in Coulomb/N or m/Volt), which express the polarization per unit force at constant electric field or the strain per unit electric field at constant stress, the dielectric constant which relates the areal charge to the applied electric field in a dielectric material, and the mechanical stiffness matrix. There are some high-power piezoelectric ceramics, such as PZT (d_{31} = 190-320 pm V^{-1}), whereas polymers such as PVDF offer lower piezoelectric power (d_{31} = 10-20 pm V^{-1}) (Lee *et al.* 2014).

Energy storage under relatively low rate of charge is usually accomplished by batteries. Although modern lithium-ion batteries provide a good solution for other high power applications, such as automotives, they pose a serious safety risk for aircraft. At present, lithium iron phosphate (LFP) batteries are regarded as the safest Li-ion battery option (Barai *et al.* 2017) and, for this reason, this is the battery type considered in this study.

Supercapacitors are generally selected for quick bursts of charge or discharge, as in the case of piezoelectric energy harvesting from vibrations. Supercapacitors for high voltage applications, as in aircraft, have organic electrolytes that reach higher maximum voltage, around 2.7 V for electrolyte 1 M TEABF$_4$ in an organic solvent (Fields *et al.* 2016, Vermisoglou *et al.* 2015a) than aqueous electrolytes. A high conductivity and low viscosity organic solvent is acetonitrile (Fields *et al.* 2016) but, due to its volatility, propylene carbonate is the preferred solvent (Lei and Lekakou 2013, Vermisoglou *et al.* 2015b) or a gel electrolyte (Lekakou *et al.* 2011) for aerospace applications.

The investigation starts with the estimation of the required power and energy for an electrified flaps actuator system for the ATR 72 aircraft, and proceeds with the evaluation of different

alternative energy harvesting systems, including solar, thermoelectric and piezoelectric energy harvesting. Appropriate energy storage systems are designed for each energy harvesting option. The final discussion compares the presented energy harvesting options and also considers combination of more than one options.

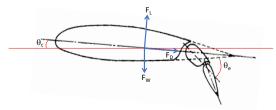## 2. Power system for flap actuators

Electromechanical actuators are smaller, lighter, less complex and more efficient than hydraulic actuators. An example of an aileron actuator for the F-18 aircraft systems reported by Jensen *et al*. (2000) was specified to have a maximum current draw of 30 A at 270 V dc, with a short pulse current peak of 70 A. The ATR 72 aircraft has four trailing edge, double-slotted flaps, two inner flaps of estimated dimensions $L_f = 0.45$ m, $b_f = 2.86$ m, $t_f = 0.11$ m and two outer flaps of estimated dimensions $L_f = 0.45$ m, $b_f = 5.73$ m, $t_f = 0.11$ m. Considering a climbing or landing angle $\theta_c = 5°$, the lift and drag force act on the wing aerofoil, as is presented in Fig. 1(a), and they are raised upon the extension of the flaps by an extension angle θ_e, where $\theta_e = 15\,°$ during takeoff and $\theta_e = 30\,°$ during landing of ATR 72 aircraft. For the maximum takeoff weight of 22500 kg for ATR 72, a specific weight of 16 kg m^{-2} is estimated for double-slotted flaps (Torenbeek 1982), which means a weight of 202 N for each inner flap and 405 N for each outer flap. The lift and drag forces, F_L and F_D, respectively, are given by the following equations:

$$F_L = \frac{1}{2} C_L \rho V^2 A \tag{1}$$

$$F_D = \frac{1}{2} C_D \rho V^2 A \tag{2}$$

where ρ is the air density taken as $\rho = 1.2235$ kg m^{-3} (interpolated between the altitudes of sea level and 7620 m, the service ceiling of ATR 72 aircraft), V is the aircraft speed taken as V = 87 m s^{-1} for climbing and landing, A is the wing area taken as 61 m^2 for ATR 72 aircraft (or the flap area for the calculations of the flap actuation power), and C_L and C_D are the lift and drag coefficients, which vary as a function of the flap extending angle (Nita 2008) as described in Fig. 1(b).

Using Eqs.(1) and (2), the ATR 72 flap dimensions and the coefficient values in Fig. 1(b), the lift and drag force on the flap are calculated for different flap extension angles and also presented

θ_e (º)	C_L	C_D	$F_{L,f}$ (kN)	$F_{D,f}$ (kN)
0	1.1	0.065	6.5, **13.1**	0.4, **0.8**
15	1.6	0.15	9.5, **19.1**	0.9, **1.8**
30	2	1.5	11.9, **23.9**	8.9, **17.9**

(a) Wing airfoil of climbing aircraft with double slotted flap; weight, lift and drag force acting on the airfoil

(b) Variation of the lift and drag coefficients as a function of the extending angle of double slotted flaps (Nita 2008) as well as the lift and drag forces on the inner flap and outer flap for different extension angles

Fig. 1 Slotted flap on wing airfoil and forces affected by the extending angle of the flap

in Fig. 1(b). Resolving the total force, force F_{ll} acts parallel to the flap and as centrifugal force, creating an angular velocity, ω_f, as the flap extends, which is given by the relation:

$$\omega_f = \frac{1}{2\pi} \sqrt{\frac{F_{ll}}{m_f L_f}} \tag{3}$$

where m_f is the flap mass. The torque on the flap, T_f, is given as a function of the total force normal to the flap, $F_\perp$, according to the equation:

$$T_f = F_\perp \frac{L_f}{2} \tag{4}$$

Given that the power, P_f, is the product of the torque and the angular velocity, Eqs. (3) and (4) yield:

$$P_f = F_\perp \frac{L_f}{4\pi} \sqrt{\frac{F_{ll}}{m_f L_f}} \tag{5}$$

Using Eq. (5) it was estimated that an inner flap requires $P_f = 1.8$ kW and 5.9 kW to extend to 15° and 30°, respectively, and an outer flap requires $P_f = 3.6$ kW and 11.9 kW to extend to 15° and 30°, respectively. Hence, 10.8 kW is needed for all four flaps during takeoff and 35.6 kW is needed for all four flaps during landing. Assuming that the flaps are airborne for 3 minutes during their operation, the energy required is 540 Wh for takeoff and 1780 Wh for landing.

Each flap actuator is designed to operate at 270 V dc and be fed by an energy storage system connected in parallel with each or pairs or all four flap actuators. Assuming LFP batteries of 90 Wh kg^{-1} operating at 1 C (Nitta *et al.* 2015, Vega-Garita *et al.* 2019), a battery mass of 26 kg is needed to store the energy required for the four flaps during a journey. However, such battery operating at 1 C would be able to deliver only 2.3 kW; a much greater battery mass of 396 kg is required to deliver the maximum power of 35.6 kW required for the four flap actuators, hence, the power delivery requirement is the dominant factor in defining the specification for the battery mass.

Considering a high energy density supercapacitor of 10 Wh kg^{-1} and 1 kW kg^{-1} (Fields *et al.* 2016), a mass of 232 kg would be needed to satisfy the energy storage requirement, which is the dominant factor for such a supercapacitor. Such a supercapacitor would self-discharge by 2% within a 60 minute period (Lei *et al.* 2020). However, it would be safer than a Li-ion battery and 59% of its weight, hence, a supercapacitor of 232 kg is recommended for the energy storage and power delivery to the four flaps.

3. Solar energy harvesting and storage

Considering the service ceiling of 7.62 km for the ATR 72 aircraft as the altitude during most of the flight time, a maximum light irradiance of 1050 W m^{-2} is assumed at such high altitude (Oumbe and Waldn 2009). Employing thin film solar panels of 10% efficiency and areal density of 2.14 kg m^{-2} (Kim *et al.* 2012) covering the upper area of each wing (61 m^2 for ATR 72), 122 m^2 total PV area of a mass of 261 kg operates at a maximum power of 12.8 kW which produces an estimated energy $E_S = 12.8$ kWh for the median journey time of 60 minutes (Jux *et al.* 2018), on the assumption that sunlight radiates at its maximum value during the whole journey. This constitutes 5.5-fold the energy specified for the four flaps operation during the takeoff and landing

phases of the journey, hence, the solar energy harvesting system may also cover other energy needs of the aircraft. The alternative producing half this energy value is also considered: $E_{S,0.5}$ = 6.4 kWh for various reasons, such as not all journey is carried out at the service ceiling and is highly clouded at lower altitudes.

A larger energy storage system may be considered for the harvested solar energy than the estimated supercapacitor for the four flaps in section 2. Considering LFP batteries of 90 Wh kg^{-1} operating at 1 C (Nitta *et al*. 2015, Vega-Garita *et al*. 2019), a battery mass of 142 kg is needed to store the maximum energy harvested during a journey E_S = 12.8 kWh. However, such battery operating at 1 C would be able to deliver only 12.8 kW; a greater battery mass of 395 kg is required to deliver the power of 35.6 kW required for the four flap actuators, hence, the power delivery requirement is the dominant factor in defining the specification for the battery mass.

Considering a high energy density supercapacitor of 10 Wh kg^{-1} and 1 kW kg (Fields *et al*. 2016), a mass of 1280 kg would be needed to satisfy the energy storage requirement, which is the dominant factor for such a supercapacitor. This is much higher than the battery mass required, hence, in this case an LFP battery of 395 kg is recommended to store the harvested energy when the solar energy system operates at its maximum capacity. Even if the solar energy system operates at half of its maximum capacity, $E_{S,0.5}$ = 6.4 kWh, the same mass of LFP battery is required for the energy storage, as the mass calculation was based on the power delivery requirement to the flaps, which remains the same.

4. Thermoelectric energy harvesting and storage

The power, P_T, of a thermoelectric generator (TEG) is given by (Pope and Lekakou 2019):

$$P_T = a\,\Delta T\,I - R\,I^2 \tag{6}$$

where I is the current, ΔT is the temperature difference between the hot side and cold side, α is the Seebeck coefficient and R is the internal resistance of the thermoelectric device. P_T acquires a maximum value, according to Eq. (6) at an optimum current, I_{opt}:

$$I_{opt} = \frac{\alpha\Delta T}{2R} \tag{7}$$

Fig. 2(a) displays the altitude profile estimated for a median flight of ATR 72 (Jux *et al*. 2018), considering a rate of climb of 6.88 m s^{-1} to the service ceiling of 7.62 km (maximum 9.14 m s^{-1} for ATR 72), cruise time of 60 minutes (Jux *et al*. 2018) and a descent rate of 7.62 m s^{-1} (data from ATR-72-200ATR –ICAO 1960). Using the following equation applied in the troposphere, i.e., for altitudes below 11 km (Earth Atmosphere Model, NASA 2014):

$$T = \frac{5}{9}(27 - 0.01168h) \tag{8}$$

where T is the temperature (ºC) and h is the altitude (m), and considering a cabin temperature of 25ºC, the hot-cold temperature difference, ΔT, profile can be calculated during the flight and the results are presented in Fig. 2(a).

A HZ-9 TEG module is considered in this investigation, of 110 g mass, with dimensions 64x64x6.6 mm, consisting of 97 [Bi,Sb)$_2$(Te,Se)$_3$] p-n couples with a device Seebeck coefficient α=378 μV K^{-1} and internal resistance R = 9.66 mΩ. If the lower surface of each wing is covered with HZ-9 TEG modules, a total surface area of 122 m^2, a total of 29785 HZ-9 TEG modules of

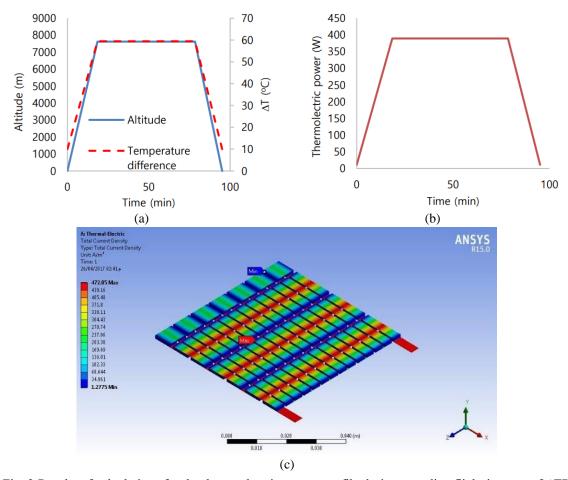(a)   (b)

(c)

Fig. 2 Results of calculations for the thermoelectric energy profile during a median flight journey of ATR 72 aircraft: (a) altitude and hot-cold temperature difference profiles, (b) total thermoelectric power profile for 29785 HZ-9 TEG modules and (c) results of simulations using ANSYS for a HZ-9 TEG module on ATR 72 at cruise altitude

3276 kg mass will be employed. Using Eqs. (6) and (7) and the temperature profile in Fig. 2(a), the maximum thermoelectric power profile is estimated and presented in Fig. 2(b). Integrating this power profile yields a total thermoelectric energy of 392.4 Wh from just the lower total surface of the wings. The optimum current and power results using Eqs. (6) and (7) were confirmed by the results of steady-state, thermal-electric conduction simulations at different ΔT values, using ANSYS; Fig. 2(c) shows the predicted current density contours in a HZ-9 TEG module at cruise altitude.

Considering LFP batteries of 90 Wh kg^{-1} operating at 1 C (Nitta *et al*. 2015, Vega-Garita *et al*. 2019), a battery mass of 4.4 kg is needed to store the energy harvested during a journey at 389 W charge power. However, such battery would not be able to discharge at 35.6 kW (90 C rate of discharge) to power the four flaps during landing. Using the supercapacitor of 232 kg recommended in section 2, could power the four flaps at 35.6 kW and also store 392.4 Wh of the thermoelectric energy harvested during a journey.

5. Piezoelectric energy harvesting and storage

5.1 Theoretical analysis of the vibrations of a cantilever beam and the piezoelectric power and energy

Islam *et al*. (2015) related the high vibration areas of an aircraft to the surfaces on which the air pressure is high, which in their simulations were identified as the lower surfaces of the wings and the fuselage. In the present study, each aircraft wing is considered as a cantilever beam under the engine weight force, as illustrated in Fig. 3(a). The beam vibrates at its natural frequencies, $f_{ni} = \omega_{ni}/2\pi$, given by the relation:

$$\omega_{ni} = \beta_i^2 \sqrt{\frac{EI}{\rho A}} \tag{9}$$

where A is the beam cross-sectional area, I is the area moment of inertia of the beam, E is the Young's modulus, ρ is the density and β_i's are obtained from the characteristic equation (Mineto *et al.* 2010):

$$\cos(\beta_i L) \cos h(\beta_i L) = -1 \tag{10}$$

The Euler-Bernoulli equation for the undamped motion of a cantilever beam under a force F expresses the beam transverse displacement (in the z axis) as a function of the position x and time t, w(x,t), as follows:

$$\rho A \frac{\partial^2 w(x,t)}{\partial t^2} + EI \frac{\partial^4 w(x,t)}{\partial x^4} = F(t)\delta(x - L_F) \tag{11}$$

where $\delta(x-L_f)$ is the Dirac delta function at $x-L_F$ and the harmonic force F, applied at distance L_F, can be expressed as a sinusoidal function:

$$F(t) = F_o \sin(\omega t) \tag{12}$$

Eq. (11) has a general solution:

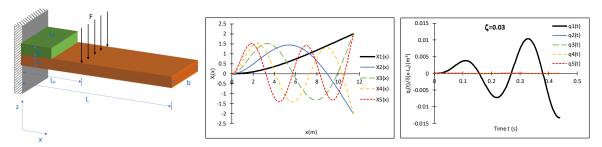$$w(x,t) = \sum_{i=1}^{n} X_i(x)\, q_i(t) \tag{13}$$

with decoupled x-position and time dependent terms: $X_i(x)$ is the i-th mode shape and $q_i(t)$ is the i-th modal coordinate function, the i-th mode corresponding to the i-th frequency ω_i. The mode shape equation, taking into account the boundary conditions, is given by:

$$X_i(x) = \cosh(\beta_i x) - \cos(\beta_i x) - \frac{\sinh(\beta_i L) - \sin(\beta_i L)}{\cosh(\beta_i L) + \cos(\beta_i L)}(\sinh(\beta_i x) - \sin(\beta_i x)) \tag{14}$$

The i-th modal coordinate equation is as follows, also taking into account damping of vibrations:

$$q_i(t) = \frac{1}{\omega_{di}} e^{-\zeta \omega_{ni} t} \frac{F_o}{\rho A} \delta(x - L_F) \int_0^t \sin(\omega \tau) e^{\zeta \omega_{ni} \tau} \sin(\omega_{di}(t - \tau))\, d\tau \tag{15}$$

where ω is the first natural frequency and the damped frequencies, ω_{di} (in rad s^{-1}) or f_{di} (in Hz), are given by the relation:

(a) Cantilever model of aircraft wing with a local load F and a piezoelectric device

(b) The first five mode shapes, $X_i(x)$

(c) The first five modal coordinate functions

Fig. 3 Cantilever model and results of the vibrations of ATR 72 aircraft wing for the first five frequencies of vibration

Table 1 Dimensions and properties of the cantilever beam (representing a wing of ATR 72) and a piezoelectric device

	Length, L (m)	11.45
	Width, b (m)	2.25
	Thickness, t (m)	0.57
Carbon fiber composite beam (Wing)	Density, ρ (kg m^{-3})	1760
	Young's modulus, E (GPa)	74
	L_F (m)	4.05
	F_o (N) (engine weight)	480.8 g[*]
	Damping ratio, ζ	0.03
	Length, L_P (m)	1
	Width, b (m)	2.25
Piezoelectric device PZT (PIC 255)	Thickness, t_P (m)	0.01
	Piezoelectric coupling coefficient, e_{31} (C m^{-2})	11.2[**]
	Permittivity, $\varepsilon_r \varepsilon_o$ (F m^{-1})	1.55x10^{-8} (PI Ceramic)
	Density (kg m^{-3})	7800

* g=9.81 m s^{-2}

**$e_{31} = E_p d_{31}$, Young's modulus of PZT PIC 255 material E_p = 62.1 GPa (Trindade and Benjeddou 2009), piezoelectric charge constant d_{31} = -180x10^{-12} C N^{-1} (PI Ceramic)

$$\omega_{di} = \omega_{ni}\sqrt{1-\zeta^2} \quad f_{di} = f_{ni}\sqrt{1-\zeta^2} \tag{16}$$
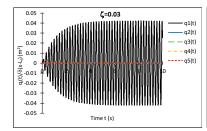
where ζ is the damping ratio.

The gradient of the beam's deflection with respect to x, $\phi(x,t)$, as a function of position x and time t is given by the relation:
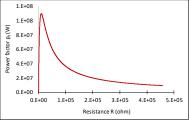
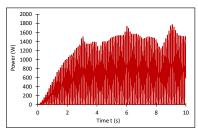$$\phi(x,t) = \frac{\partial \sum_{i=1}^{n} X_i(x) q_i(t)}{\partial x} \tag{17}$$

Table 2 Natural frequencies and frequency parameters for the vibrating cantilever beam-modeled wing of the ATR 72 aircraft

$\beta_i L$	β_i (m^{-1})	f_{ni} (Hz)	ω_{ni} (rad s^{-1})
1.875	0.1637	4.57	28.7
4.694	0.4099	28.63	180
7.855	0.6860	80.17	503
10.996	0.960	157.10	987
14.14	1.2349	259.78	1630

(a) The first five modal coordinate functions during the first 10 seconds

(b) Resistance optimization by maximizing power factor

(c) The piezoelectric power profile of a cantilever beam-modeled wing of the ATR 72 aircraft

Fig. 4 Simulation results for the prediction of the piezoelectric power from the vibrations of a cantilever beam-modeled wing of the ATR 72 aircraft

Eq. (17) determines the current, I, passing through the piezoelectric device of dimensions L_P, b and t_P according to the equation (Fu *et al* 2018, Khalatkar *et al*. 2014):

$$I(t) = \frac{\omega b(t+t_p)e_{31}[\phi(0,t)-\phi(L,t)]}{2\left(1+bL_P\varepsilon_r\varepsilon_o\frac{\omega R}{t_P}\right)}$$

(18)

The piezoelectric power generated by the piezoelectric device on each wing, P_{P1}, is then given by the relation:

$$P_{P1} = I^2 R$$

(19)

where R is the external resistance load that can be optimized to maximize the power delivered by the piezoelectric devices.

5.2 Simulations of the vibrating wing and results of the piezoelectric power and energy

Table 1 contains the dimensions and properties of the cantilever beam and the piezoelectric device used in the piezoelectric power and energy simulations of this study. The cantilever beam represents each wing of the ATR 72 aircraft with general properties of a carbon fiber composite material. The piezoelectric device material is PZT PIC 255 (from PI Ceramic) with property values obtained from their product catalogue.

The first five solutions $\beta_i L$ of Eq. (10) and the associated natural frequencies, f_{ni} given by Eq. (9) are presented in Table 2. Substituting the β_i values from Table 2 in Eq. (14), the first five mode

shapes, $X_i(x)$, are predicted and presented in Fig. 3(b). It can be seen that $X_1(x)$ yields maximum displacement at the tip of the beam-modeled wing, x=L, $X_2(x)$-$X_5(x)$ have a significant effect on the beam-modeled wing at the position of the engine weight, x=L_f, $X_4(x)$ and $X_5(x)$ have a significant effect in the region of the piezoelectric device. Employing Eq.(15), the first five modal coordinate functions are predicted and presented in Fig. 3(c) where the presented $q_i(t)/\delta(x-L_f)$ functions include the harmonic effect but not the localized effect of the external force. Fig. 3(c) shows clearly that the first modal coordinate function, $q_1(t)/\delta(x-L_f)$, is dominant and the rest of the $q_i(t)/\delta(x-L_f)$ functions, at higher frequencies, have negligible effect: for example, peak ratio $q_1(t)/q_2(t) = 54$ in the first period and peak ratio $q_1(t)/q_2(t) = 173$ in the second period, with the modal coordinate function peaks becoming lower as the frequency increases.

Fig. 4(a) presents the modal coordinate functions for longer duration, i.e., during the first 10 seconds, where it can be seen that the damping takes effect by stabilizing the oscillation amplitude after about 3.15 s. The next step is to optimize the resistance, R, by maximizing the power factor, p_f:

$$p_f = R \left[\frac{\omega b(t + t_p)e_{31}}{2\left(1 + bL_P\varepsilon_r\varepsilon_o \frac{\omega R}{t_P}\right)} \right]^2 \tag{20}$$

Fig. 4(b) presents the power factor as a function of resistance, with the maximum p_f value at R = 10×10^3 ohm. Employing Eqs. (18) and (19), the power profile can be predicted for a vibrating ATR 72 wing and is depicted in Fig. 4(c): power peaks at 1600-1770 W are observed. Considering a median flight time of 60 minutes (Jux *et al*. 2018), the integration of the power profile during this duration yields 1500 Wh piezoelectric energy from both wings. The energy could be stored in the 232 kg supercapacitor, which can operate at 3.5 kW, the maximum piezoelectric power from both wings during its charge, and at 35.6 kW during its discharge to power the four flaps at the peak required power.

6. Conclusions

The present investigation has considered to make the ATR 72 aircraft more electric by employing electromechanically actuated flaps to replace the four existing flaps currently hydraulically actuated. Fig. 1(b) demonstrates that double-slotted flaps have a significant effect on the drag and lift force of ATR 72 aircraft, especially for the larger extending angle $\theta_e = 30^o$ during landing. This leads to considerable energy requirements for the operation of the four flap actuators, 540 Wh for takeoff and 1780 Wh for landing, with a maximum power requirement of 35.6 kW for all four flaps during landing. It was estimated that a supercapacitor of 232 kg could provide the energy storage and power required for the four flaps, which proved to be 59% of the required weight of an LFP battery while the supercapacitor also constitutes a safer solution. Table 3 summarizes both the requirements of the power system for the electromechanical actuators of the four flaps and also the characteristics of each investigated energy harvesting solution and its associated energy storage and power delivery system which complies with the power requirements of the flaps actuators.

From the three researched energy harvesting options, solar energy harvesting using thin film photovoltaics covering the upper surface of the two wings could provide a maximum power of

Table 3 Summary of characteristics of requirements and solutions investigated to power a system of electromechanical flap actuators in ATR 72 aircraft

Requirements		Solar energy harvesting and storage system		Thermoelectric harvesting and storage system		Piezoelectric harvesting and storage system	
Power for flaps during takeoff (kW)	10.8	Power delivery by battery (kW)	35.6	Power delivery by supercapacitor (kW)	35.6	Power delivery by supercapacitor (kW)	35.6
Power for flaps during landing (kW)	35.6						
Energy for flaps during takeoff (Wh)	540	Max harvested energy in median journey (Wh)	12800	Max harvested energy in median journey (Wh)	392	Max harvested energy in median journey (Wh)	1500
Energy for flaps during landing (Wh)	1780						
		LFP battery mass (kg) for energy storage and power delivery	395	Supercapacitor mass (kg) for energy storage and power delivery	232	Supercapacitor mass (kg) for energy storage and power delivery	232
		Mass of PVs (kg)	261	Mass of TEGs (kg)	3276	Mass of piezoelectric devices (kg)	351
		Total mass of energy harvesting & storage/power system (kg)	656	Total mass of energy harvesting & storage/power system (kg)	3508	Total mass of energy harvesting & storage/power system (kg)	583

12.8 kW and a maximum energy of 12.8 kWh for the median journey time of 60 minutes (Jux *et al*. 2018), if it is considered that the maximum sunlight irradiance takes place during the whole journey for the particular geographical region at the most suitable time of the day and the year. This constitutes 5.5-fold the energy specified for the four flaps operation during the takeoff and landing phases of the journey, hence, the solar energy harvesting system at its maximum power and capacity may also cover other energy needs of the aircraft. However, if the journey takes place during the night or during times of lower solar irradiance for the particular geographical region and the temporal position of the sun, no or much less solar energy would be harvested. The energy storage system to be selected may depend on the journey schedule and geographical region of the journeys of a particular aircraft. If the solar energy harvesting system operates at its maximum capacity for most of the journey, an LFP battery of 395 kg has been recommended. Otherwise, the 232 kg supercapacitor proposed for powering the four flaps would be also appropriate for storing the harvested solar energy. Given the low weight of the thin film PVs, this solution has relatively low total mass for both the energy harvesting and storage system, compared to the piezoelectric energy harvesting system, and offers the potential of the highest energy density system (Wh per kilogram) if the journey is such that the solar energy harvesting system operates at its maximum capacity.

Thermoelectric modules covering the lower surface of the two wings were estimated to be able to produce 392 Wh at a power of 389 W during a median journey of ATR 72 aircraft. This is 17% of the energy required for the four flaps of ATR 72 aircraft during a median journey, which could be stored in the 232 kg supercapacitor recommended to power the four flaps at 35.6 kW maximum power. As seen in Table 3, due to the high weight of TEG modules, this is the highest mass and the lowest energy density solution and could only be recommended if novel thermoelectric materials had dual role, structural and thermoelectric, in dual functionality wings of the future, in which the structural mass is reduced and replaced by thermoelectric mass.

Piezoelectric energy harvesting derived from wing vibrations generates power peaks of 1600-1770 W from each wing and a total energy of 1500 Wh from both wings during a median flight time of 60 minutes (Jux *et al.* 2018). This constitutes 65% of the energy required for the four flaps of ATR 72 aircraft during a median journey, which could be stored in the 232 kg supercapacitor recommended to power the four flaps at 35.6 kW maximum power. As seen in Table 3, this constitutes the lowest total mass solution, including the mass of both the energy harvesting and storage devices.

Overall, a combination of piezoelectric and thermoelectric energy harvesting can supply 82% of the energy required for the operation of the electromechanically actuated flaps. The remaining 18% energy can be harvested by photovoltaics. All harvested energy can be stored in a 232 kg supercapacitor which can deliver this energy to the flap actuators during takeoff and landing at the maximum power of 35.6 kW. Any excess of solar energy harvested may be used immediately by systems operating in flight, without any need for storage.

In conclusion, a 232 kg supercapacitor is recommended for the energy storage and power system in this study, which has many advantages compared to an LFP battery: better weight-related performance, superior safety, no need for high demand/high cost lithium material, and better recyclability than a battery by disassembly and materials separation via washing, dissolution, filtering and dielectrophoresis (Vermisoglou *et al* 2016, Kampouris *et al* 1987, Kampouris *et al* 1988).

References

André, C., Vasilevskiy, D., Turenne, S. and Masut, R.A. (2009), "Extruded bismuth-telluride-based n-type alloys for waste heat thermoelectric recovery applications", *J. Electron. Mater.*, **38**(7), 1061-1067. https://doi.org/10.1007/s11664-009-0695-5.

ATR (1999), *ATR 72 Flight Crew Operating Manual*, ATR Training Center.

ATR (2010), *ATR Systems: ATR Flight and Operation Services*, ATR, Blagnac, France.

Barai, A., Uddin, K., Chevalier, J., Chouchelamane, G.H., McGordon, A., Low, J. and Jennings, P. (2017), "Transportation safety of lithium iron phosphate batteries - a feasibility study of storing at very low states of charge", *Sci Rep.*, **7**(1), 1-10. https://doi.org/10.1038/s41598-017-05438-2.

Fields, R., Lei, C., Markoulidis, F. and Lekakou C. (2016), "The composite supercapacitor", *Energy Technol.*, **4**(4), 517-525. https://doi.org/10.1002/ente.201500328.

Fu, H., Chen, G. and Bai, N. (2018), "Electrode coverage optimization for piezoelectric energy harvesting from tip excitation", *Sensors*, **18**(3), 804, 1-14. https://doi.org/10.3390/s18030804.

Hudson, O.A., Fanni, M., Ahmed, S.M. and Sameh, A. (2020), "Autonomous flight take-off in flapping wing aerial vehicles", *J. Intell. Robot. Syst.*, **98**(1), 135-152. https://doi.org/10.1007/s10846-019-01003-3.

ICAO (1996), ATR-72-200ATR - AT72 L2T M - Doc8643, https://doc8643.com.

Islam, T., Alam, S., Rahman, T. and Hasan, M. (2015), "Power harvesting from aircraft body using piezoelectric material", *Proceedings of the 10th Global Engineering, Science and Technology Conference*,

Dhaka, Bangladesh, January.

Jensen, S.C., Jenney, G.D., Raymond, B. and Dawson, D. (2000), "Flight test experience with an electromechanical actuator on the F-18 systems research aircraft", *Proceedings of the 19th Digital Avionics Systems Conference*, Philadelphia, Pennsylvania, U.S.A., October.

Jux, B., Foitzik, S. and Doppelbauer, M. (2018), "A standard mission profile for hybrid-electric regional aircraft based on web flight data", *Proceedings of the 2018 IEEE International Conference on Power Electronics, Drives and Energy Systems (PEDES)*, Chennai, India, December.

Kampouris, E.M., Papaspyrides, C.D. and Lekakou, C.N. (1987), "A model recovery process for scrap polystyrene foam by means of solvent systems", *Conserv. Recycling*, **10**(4), 315-319. https://doi.org/10.1016/0361-3658(87)90062-2.

Kampouris, E.M., Papaspyrides, C.D. and Lekakou, C.N. (1988), "A model process for the solvent recycling of polystyrene", *Polym. Eng. Sci.*, **28**(8), 534-537. https://doi.org/10.1002/pen.760280808.

Khalatkar, A., Gupta, V.K. and Agrawal, A. (2014) "Analytical, FEA, and experimental comparisons of piezoelectric energy harvesting using engine vibrations", *Smart Mater. Res.*, 1-8. http://doi.org/10.1155/2014/741280.

Kim, H.C., Fthenakis, V., Choi, J.K. and Turney, D.E. (2012), "Life cycle greenhouse gas emissions of thin-film photovoltaic electricity generation", *J. Industr. Ecol.*, **16**(S1), S110-S121. https://doi.org/10.1111/j.1530-9290.2011.00423.x.

Lee, H.J., Zhang, S., Bar-Cohen, Y. and Sherrit, S. (2014), "High temperature, high power piezoelectric composite transducers", *Sensors*, **14**(8), 14526-14552. https://doi.org/10.3390/s140814526.

Lei, C. and Lekakou, C. (2013), "Activated carbon-carbon nanotube nanocomposite coatings for supercapacitor application", *Surf. Coat. Tech.*, **232**, 326-330. https://doi.org/10.1016/j.surfcoat.2013.05.027.

Lei, C., Fields, R., Wilson, P., Constantina Lekakou, C., Amini, N., Tennison, S., Perry, J., Gosso, M. and Martorana, B. (2020), "Development and evaluation of a composite supercapacitor-based 12 V transient start-stop (TSS) power system for vehicles: Modelling, design and fabrication scaling up", *Proc. Inst. Mech. Eng. Part A J. Power Energy*. https://doi.org/10.1177/0957650920930166.

Lekakou, C., Moudam, O., Markoulidis, F., Andrews, T., Watts, J.F. and Reed, G.T. (2011), "Carbon-based fibrous EDLC capacitors and supercapacitors", *J. Nanotechnol.*, 409382. https://doi.org/10.1155/2011/409382.

Lim, S.S., Kim, B.K., Kim, S.K., Park, H.H., Kim, D.I., Hyun, D.B., Kim, J.S. and Baek. S.H. (2017), "A two-step synthesis process of thermoelectric alloys for the separate control of carrier density and mobility", *J. Alloy. Compd.*, **727**, 191-195. https://doi.org/10.1016/j.jallcom.2017.08.089.

Matlock, J., Sharikov, P., Warwick, S., Richards, J. and Suleman, A. (2019), "Evaluation of energy efficient propulsion technologies for unmanned aerial vehicles", *T. Can. Soc. Mech. Eng.*, **43**(4), 481-489. https://doi.org/10.1139/tcsme-2018-0231.

Mineto, A.T., de Souza Braun, M.P., Navarro, H.A. and Varoto, P.S. (2010), "Modeling of a cantilever beam for piezoelectric energy harvesting", *Proceedings of the DINCON2010, 9th Brazilian Conference on Dynamics, Control and their Applications*, Serra Negra, Brazil, June.

Moore, K.R. and Ning, A. (2019), "Takeoff and performance trade-offs of retrofit distributed electric propulsion for urban transport", *J. Aircraft*, **56**(5), 1880-1892. https://doi.org/10.2514/1.C035321.

NASA (2014), Earth atmosphere model, https://www.grc.nasa.gov/WWW/K-12/rocket/atmos.html.

Nita, M.F. (2008), "Aircraft design studies based on the ATR 72", Ph.D. Dissertation, University of Applied Sciences, Hamburg, Germany.

Nitta, N., Wu, F., Lee, J.T. and Yushin, G. (2015), "Li-ion battery materials: Present and future", *Mater. Today*, **18**(5), 252-264. https://doi.org/10.1016/j.mattod.2014.10.040.

Oumbe, A. and Wald, L. (2009), "A parameterisation of vertical profile of solar irradiance for correcting solar fluxes for changes in terrain elevation", *Proceedings of the Earth Observation and Water Cycle Science Conference*, Frascati, Italy, November.

PI Ceramic (n.d.), Piezoelectric ceramic products datasheet, Catalogue CAT 125, PI Ceramic GmbH, https://www.piceramic.com/en/products/piezoelectric-materials/#c15163.

Pope, J. and Lekakou, C. (2019), "Thermoelectric polymer composite yarns and an energy harvesting wearable textile", *Smart Mater. Struct.*, **28**(9), 095006. https://doi.org/10.1088/1361-665X/ab1cc1.

Qiao, G., Liu, G., Shi, Z., Wang, Y., Ma, S. and Lim, T.C. (2018), "A review of electromechanical actuators for More/All Electric aircraft systems", *Proc. Inst. Mech. Eng. Part C J. Mech. Eng. Sci.*, **232**, 4128-4151. https://doi.org/10.1177/0954406217749869.

Sirohi, J. and Chopra, I. (2000), "Fundamental understanding of piezoelectric strain sensors", *J. Intell. Mater. Syst. Struct.*, **11**(4), 246-257. https://doi.org/10.1106/8BFB-GC8P-XQ47-YCQ0.

Söderström, T., Haug, F.J., Terrazzoni-Daudrix, V. and Ballif, C. (2008), "Optimization of amorphous silicon thin film solar cells for flexible photovoltaics", *J. Appl. Physics*, **103**(11), 114509. https://doi.org/10.1063/1.2938839.

Torenbeek, E. (1982), *Synthesis of Subsonic Airplane Design*, Springer Science, 454.

Trindade, M.A. and Benjeddou, A. (2009), "Effective electromechanical coupling coefficients of piezoelectric adaptive structures: Critical evaluation and optimization", *Mech. Adv. Mater. Struct.*, **16**(3), 210-223. https://doi.org/10.1080/15376490902746863.

Trinklein, E.H., Cook, M.D., Parker, G.G. and Weaver, W.W. (2020), "Exergy optimal multi-physics aircraft microgrid control architecture", *Int. J. Elec. Power Energy Syst.*, **114**, 105403. https://doi.org/10.1016/j.ijepes.2019.105403.

Vega-Garita, V., Hanif, A., Narayan, N., Ramirez-Elizondo, L. and Bauer, P. (2019), "Selecting a suitable battery technology for the photovoltaic battery integrated module", *J. Power Sources*, **438**, 227011. https://doi.org/10.1016/j.jpowsour.2019.227011.

Vermisoglou, E.C., Giannakopoulou, T., Romanos, G., Giannouri, M., Boukos, N., Lei, C., Lekakou, C. and Trapalis, C. (2015a), "Effect of hydrothermal reaction time and alkaline conditions on the electrochemical properties of reduced graphene oxide", *Appl. Surf. Sci. Part A*, **358**, 100-109. https://doi.org/10.1016/j.apsusc.2015.08.127.

Vermisoglou, E.C., Giannakopoulou, T., Romanos, G.E., Boukos, N., Giannouri, M., Lei, C., Lekakou, C. and Trapalis, C. (2015b), "Non-activated high surface area expanded graphite oxide for supercapacitors", *Appl. Surf. Sci. Part A*, **358**, 110-121. https://doi.org/10.1016/j.apsusc.2015.08.123.

Vermisoglou, E.C., Giannouri, M., Todorova, N., Giannakopoulou, T., Lekakou, C. and Trapalis, C. (2016), "Recycling of typical supercapacitor materials", *Waste Manage. Res.*, **34**(4), 337-344. https://doi.org/10.1177/0734242X15625373.

Voskuijl, M., van Bogaert, J. and Rao, A.G. (2018), "Analysis and design of hybrid electric regional turboprop aircraft", *CEAS Aeronaut. J.*, **9**(1), 15-25. https://doi.org /0.1007/s13272-017-0272-1.

Xu, L., Liu, Y., Chen, B., Zhao, C. and Lu, K. (2013), "Enhancement in thermoelectric properties using a p-type and n-type thin-film device structure", *Polym. Compos.*, **34**(10), 1728-1734. https://doi.org/10.1002/pc.22576.

AP